Available online at www.sciencedirect.com
ScienceDirect
Journal of Solid State Chemistry 180 (2007) 3360–3365
JOURNAL OF SOLID STATE CHEMISTRY
www.elsevier.com/locate/jssc

Synthesis and electrochemical performances of amorphous carbon-coated Sn–Sb particles as anode material for lithium-ion batteries

Zhong Wang[a,b], Wenhuai Tian[c], Xiaohe Liu[d], Rong Yang[a], Xingguo Li[a,*]

[a]*State Key Laboratory of Rare Earth Materials Chemistry and Applications, College of Chemistry and Molecular Engineering, Peking University, Beijing 100871, China*
[b]*General Research Institute for Nonferrous Metal, Beijing 100088, China*
[c]*Department of Materials Physics and Chemistry, University of Science and Technology Beijing, Beijing 100083, China*
[d]*Department of Inorganic Materials, Central South University, Changsha, Hunan 410083, China*

Received 5 June 2007; received in revised form 11 September 2007; accepted 2 October 2007
Available online 5 October 2007

Abstract

The amorphous carbon coating on the Sn–Sb particles was prepared from aqueous glucose solutions using a hydrothermal method. Because the outer layer carbon of composite materials is loose cotton-like and porous-like, it can accommodate the expansion and contraction of active materials to maintain the stability of the structure, and hinder effectively the aggregation of nano-sized alloy particles. The as-prepared composite materials show much improved electrochemical performances as anode materials for lithium-ion batteries compared with Sn–Sb alloy and carbon alone. This amorphous carbon-coated Sn–Sb particle is extremely promising anode materials for lithium secondary batteries and has a high potentiality in the future use.

Keywords: Composite materials; Electrode materials; Coating materials; Metals and alloys

1. Introduction

Tin-based alloys have been considered as an attractive replacement for graphite anodes in lithium-ion battery systems due to their superior lithium storage capacity. However, tin-based alloys have not been applied to commercial lithium-ion batteries due to the mechanical disintegration of active materials caused by a large volume change during charge–discharge processes [1–3]. In order to solve these problems, multi-phase composite structures and small particle alloy systems have been proposed [4–6]. The decreased particle size can greatly increase the morphology stability. However, due to the huge specific surface energy, ultrafine active materials may cause the server aggregation [7–10]. The cycling performance of nanosized metal particles can be improved by composite of the metal and carbon, where the carbon acts as a barrier to prevent the aggregation between the metal particles, and provides a void space where the metal particles experience a volume change [11–14]. Several alloy and composite material such as "alloy-coated carbon" [15–23], "carbon-coated alloy" [13,24–28] have been utilized to solve the above intractable problem for the metal-based materials. For instance, Li et al. [17] reported that dispersing nano-sized SnSb alloy on the surface of hard carbon spherules (HCS) is an effective way to enhance the dimensional stability of nano-alloy particles during Li insertion and extraction. Wang [23] synthesized the tin/graphite composite material by mechanical milling of tin and graphite, and the composite anode revealed a reversible capacity of 800–1250 mAh g^{-1} within 20 cycles, however, it shows a larger irreversible capacity loss. Lee et al. [13] have reported that the Sn-encapsulated spherical hollow carbon composites was synthesized for raw materials with cetyltrimethylammonium bromide (CTAB, as a surfactant), the mixture of resorcinol and formaldehyde (RF, as a carbon source), tributylphenyltin (TBPT, as a Sn source) to

*Corresponding author. Fax: +86 10 6276 5930.
E-mail address: xgli@pku.edu.cn (X. Li).

0022-4596/$ - see front matter © 2007 Elsevier Inc. All rights reserved.
doi:10.1016/j.jssc.2007.10.002

obtain surfactant-stabilized TBPT/RF core–shell colloids followed by high temperature carbonization. The spherical hollow carbon acts as a barrier to prevent the aggregation between Sn particles and carbon provides a void space where Sn metal particles experience a volume change without a collapse of carbon shell.

Recently, we succeeded in synthesizing Sn–Sb nanoparticles by hydrogen plasma-metal reaction method. The Sn–Sb nanoparticles show better morphology stability than the micro-size materials [29,30]. In this study, the amorphous carbon-coated Sn–Sb nanoparticles composite material was obtain with high capacity and good cycle performance by a simple and effective hydrothermally treated method, and their electrochemical properties as an alternative anode material for lithium-ion batteries were investigated.

2. Experimental

2.1. Preparation and characterization of specimen

Sn–Sb nanoparticles were prepared: the Sn–Sb ingots were prepared from 99.9 wt% purity Sn (30 at%) and Sb (70 at%) by arc melting in an argon gas atmosphere. Arc-melted ingots were flipped over and remelted four times to get a homogeneous composition. Then Sn–Sb nanoparticles were prepared by arc melting an ingot of the Sn–Sb alloy ingots in a mixture of 80% Ar + 20% H_2 of 0.1 MPa. After passivation in an Ar + 5% O_2 atmosphere for 24 h, the nanoparticles were taken out of the arc-melting chamber [29].

Amorphous carbon-coated Sn–Sb particles (ACSP) were prepared: Glucose (0.5 g) was dissolved in distilled and deoxygenated water (20 ml) until a clear solution was observed. Then, the Sn–Sb particles (0.25 g) were dispersed in the solution under ultrasonication for 30 min. Next, adequate zinc tablets were added into solution to protect samples from oxidation. The mixture was then transferred into a 40 ml Teflon-sealed autoclave purged with the Ar and maintained at 160 °C for 4 h. After removed zinc tablets and the supernatants, the products were isolated by centrifugation and washed with deionized water and acetone three times, respectively, and dried at 120 °C under vacuum overnight. Then, the product was heat treated at 800 °C for 2 h under argon atmosphere to carbonize the sample surface.

Amorphous carbon balls were prepared: glucose (4 g) was dissolved in water (20 ml). Other steps are same with the preparation of amorphous carbon-coated Sn–Sb particles, and the sample was heat treated at 1000 °C for 2 h.

The crystal structure of the as-prepared particle samples was characterized by X-ray diffraction (XRD) using Cu$K\alpha$ radiation. The morphology, size distribution and shape of particles were observed using a JEOL 200EX transmission electron microscope (TEM) operated at 160 kV. Energy dispersive spectra (EDS) analyses were conducted on a Tecnai F30.

2.2. Electrochemical measurement

To evaluate the electrochemical characteristics, electrodes were fabricated using the powders by mixing 80 wt% active powders, 10 wt% acetylene black and 10 wt% polyvinylidene fluoride (PVDF) dissolved in *n*-methyl pyrrolidinone. The resultant slurries were spread on copper foil substrates. After coating, the electrodes were pressed and dried at 120 °C under vacuum for 24 h. Li metal foil was utilized as the counter electrode, 1 M LiPF6 in ethylene carbonate (EC) and dimethyl carbonate (DMC) (1:1 by volume) was used as the electrolyte, and Celgard 2400 was used as the separator. Half-cells were assembled in an argon-filled glove box. Unless stated otherwise, charging and discharging test was carried out under a controlled cut-off voltage from 0 to 1.5 V and at a constant current density of 50 mA g^{-1}.

3. Results and discussion

3.1. Microstructure of ACSP

The reddish brown products formed when a glucose solution blended Sn–Sb particles were hydrothermally treated below 160 °C for 4 h. The color of product becomes black after heat treated at 800 °C for 2 h.

Fig. 1 shows the XRD patterns of the amorphous carbon-coated Sn–Sb particles (ACSP). For comparison, the XRD pattern of Sn–Sb alloy particles is also shown. The XRD pattern of ACSP sample before and after heat treatment shows the existence of SnSb and Sn (see Fig. 1c). This is same as the Sn–Sb alloy particles (see Fig. 1a). There is a little SnO_2 phase observed in the ACSP sample before heat treatment (see Fig. 1b). However, the SnO_2 phase disappeared after heat treatment. It indicates that the SnO_2 have been reduced during heat treatment. The graphite peak was not observed on the XRD pattern of

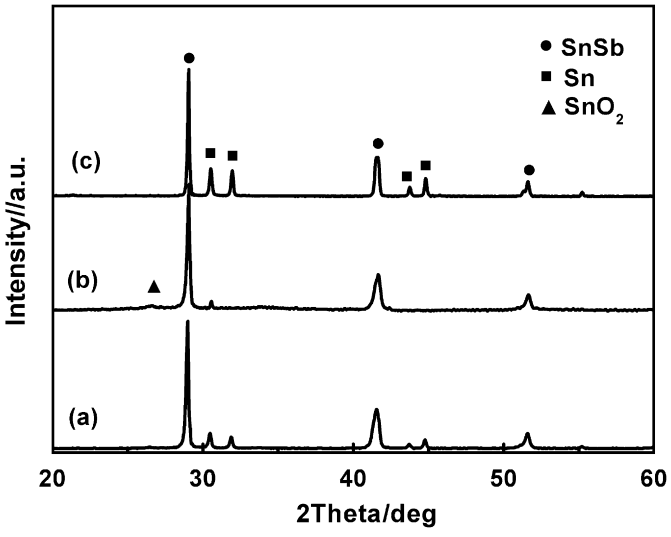

Fig. 1. X-ray diffraction patterns of (a) Sn–Sb alloy particles, (b) ACSP sample before heat treatment, (c) ACSP sample after heat treatment.

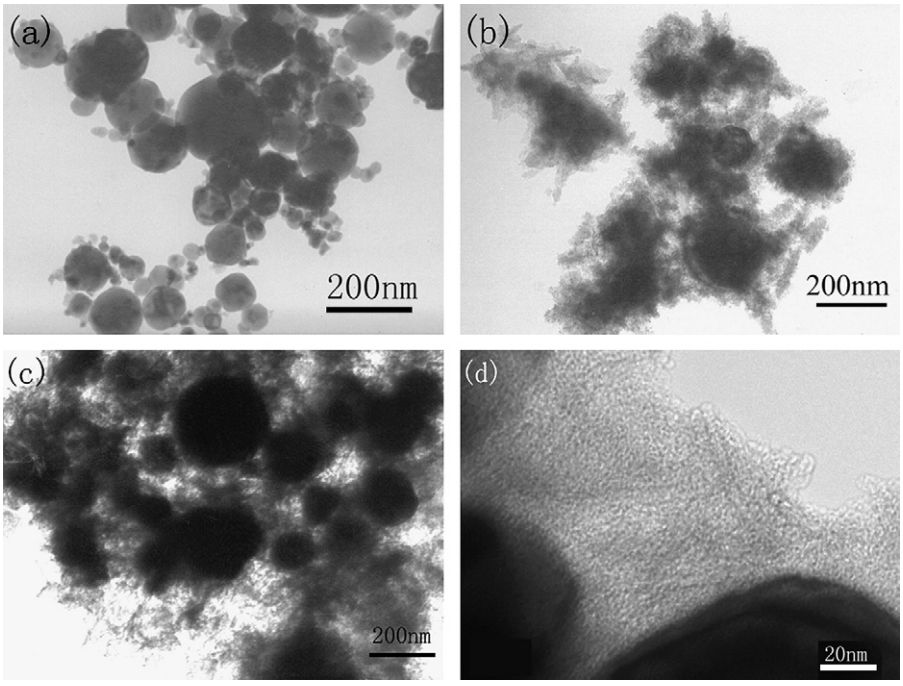

Fig. 2. TEM images of (a) Sn–Sb alloy particles, (b) ACSP sample before heat treatment, (c) ACSP sample after heat treatment, (d) and a high-magnified TEM image of ACSP samples after heat treatment.

ACSP sample either, because the carbonaceous material formed by the glucose dehydration was amorphous.

Fig. 2 shows TEM images of ACSP and the Sn–Sb particles. Fig. 2(a) shows the TEM images of Sn–Sb particles. The particles are spherical in shape and most of them have a size distribution ranging from 50 to 200 nm in diameter. Fig. 2(b) shows TEM image of the sample before the heat treatment. All the particles show a black contrast in the center that is considered as the tin antimony alloy. The amorphous carbon is surrounding the tin antimony alloy and shows a shallow contrast in the image. Fig. 2(c) shows the TEM images of ACSP samples after the heat treatment. It is clear that no obvious change in morphology and dimension has been observed for the samples that were undergone heat treatment compared with the samples without heat treatment. The melting point of tin antimony alloy is around 425 °C. When the temperature of heat treatment is 800 °C, higher than the melting point, the tin antimony alloy has melted, however it did not form a solid block after heat treatment. This fact indicates that the outer surface material played the role of containers, which prevented the melting of inner Sn–Sb alloy from flowing out, and maintained the original size and shape. Fig. 2(d) is a high-magnified TEM image of samples after heat treatment, showing the carbonaceous material coated the surface of Sn–Sb particles is a loose cotton-like structure.

The EDS profile of the ACSP sample after heat treatment is shown in Fig. 3, in which carbon, tin, antimony, oxygen and copper elements are identified. The copper peak might come from copper grid used to support the powder specimen for TEM analysis. The appearance of carbon peak strongly supports the proposition that amorphous carbon layer formed on the surface of Sn–Sb particles.

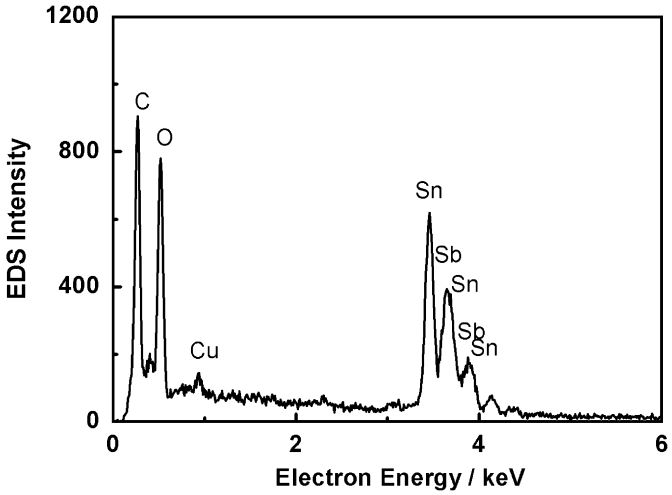

Fig. 3. EDS profile of the ACSP sample after heat treatment.

Summing up the experimental results of XRD and EDS, it can be suggested that a layer of material contained carbon formed on the surface of Sn–Sb particles after hydrothermal treatment in the glucose solution and then the layer material transform to amorphous carbon after the following heat treatment. No oxide peaks were found on the XRD pattern of ACSP sample after heat treatment, but it appeared on the EDS profile, showing that only a few oxides were on the surface of composite materials. We put

the zinc tablets into solution to protect samples from oxidation, but it is still difficult to completely avoid the appearance of oxides in hydrothermal conditions.

3.2. The formation mechanism

It was reported that the carbon spheres could be prepared from glucose under hydrothermal conditions between 160 and 180 °C. This is higher than the normal glycosidation temperature, which leads to aromation and carbonization [31–34].

As the autoclave is heated to a certain temperature, the adjacent sugar molecules in the solution start to dehydrate and polymerize (polycondensation reaction). Consequently, an amphiphilic compound with a larger hydrophobic alkyl and hydrophilic hydroxyl is formed. When the concentration reaches the critical micelle point with the polymerization of sugar molecules, the amphiphilic compound forms spherical micelles, of which the hydrophobic groups make up of the core of the micelles and the hydrophilic hydroxyls occupy the surface. After the nucleation process, the surface hydroxyls continue to react with the nearest free molecules and dehydrate, and the spherical micelle particles grows up. When the sugar molecules are exhausted, the growth of the spherical particles stops [33].

By the thermodynamics of phase transition process, the increases of surface energy in the non-homogeneous phase system was less than that in homogeneous phase system when new phase nucleated and coarsened in the existing solid surface. When some Sn–Sb alloy particles were added in the glucose solution, they will act as a nucleation center. Glucose can form crystal nucleus on these second-phase particles surface before it forms spherical micelle. Hydroxyl in the glucose can react with hydrogen atom to dehydrate on the Sn–Sb alloy particles surface, and forms gradually a coating layer on the particles surface. To form a coating layer, the sticking point is to choose the marginal value of glucose concentration between heterogeneous nucleation and homogeneous nucleation.

The carbon-coated layer of ACSP samples is not smooth but loose cotton-like. It is because that the surface form many nanometer-level crevices during the glucose dehydration and carbonization, which enables the specific surface area of carbon ball formed by the pure glucose dehydration to achieve $300\,m^2\,g^{-1}$ [34]. In addition, oxide mixes with carbon to increase the interstice due to the Sn–Sb particles oxidizing slightly during the glucose dehydration.

3.3. Electrochemical study

Fig. 4 shows the charge and discharge curves of ACSP sample (unless stated otherwise, ACSP denote the sample after heat treated) as well as those of the Sn–Sb alloy particles and amorphous carbon ball as a comparison. The first lithiation capacity and delithiation capacity of the composite materials sample non-carbonized heat treatment

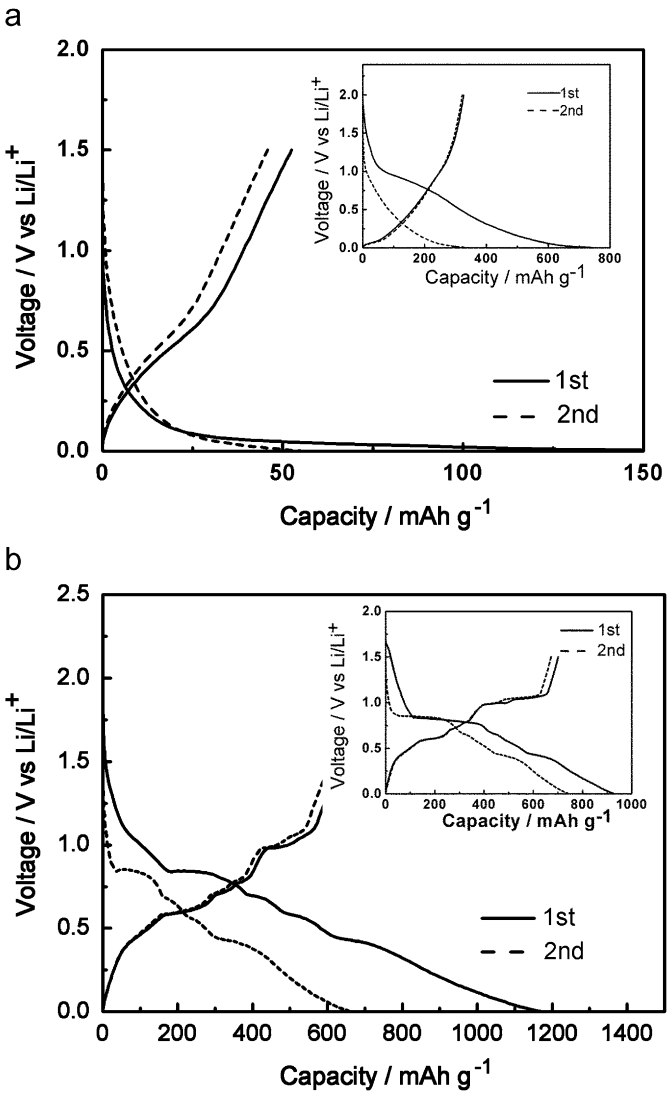

Fig. 4. The charge and discharge curve of ACSP sample, (a) before heat treatment, inset: amorphous carbon; (b) after heat treatment, inset: Sn–Sb alloy particles.

(see Fig. 4(a)) were all extremely low. Its first lithiation capacity is $160\,mAh\,g^{-1}$, and the reversible capacity is only $60\,mAh\,g^{-1}$. No Sn–Sb alloy characteristic can be found in the charge and discharge curve (see inset of Fig. 4(b)). However, it is very similar with the amorphous carbon (see inset of Fig. 4(a)), indicating that Sn–Sb alloy in the composite materials samples did not participated in the electrochemical reaction and only the coating layer of samples reacted with lithium ion.

The composite material samples are determined to be composed of Sn–Sb alloy mainly according to the XRD pattern, but Sn–Sb alloy in the sample has not participated in the electrochemical reaction, which showed that the Sn–Sb particles must be enwrapped by some materials which make lithium ion hard to traverse. It can be considered that a colloidal materials, which is a partially carbonization materials but not pure carbon has formed on

the Sn–Sb particles surface after hydrothermal treatment in the glucose solution. It could prevent the lithium ion from traversing and reacting with the Sn–Sb alloy. Therefore, the charge and discharge curve only assume the characteristics of partially carbonization material on the surface.

Fig. 4(b) shows the charge and discharge curves of composite materials sample after undergoing a heat treatment at 800 °C. The Sn–Sb alloy charge and discharge characteristic potential platform can be found obviously (see inset of Fig. 4(b)). Its first discharge capacity achieves 1173 mAh g^{-1} and the reversible capacity is 634 mAh g^{-1}. Obviously, after the heat treatment, the coating layer on the surface of Sn–Sb alloy particles already carbonized and the lithium ion can pass through to react with internal Sn–Sb alloy. However, it is clear that the irreversible capacity of the sample is bigger than that of the pure Sn–Sb alloy. This may be contributed by the loose porous properties of coating layer.

Fig. 5 shows the cycle capacity vs. cycle number of the ACSP sample as well as Sn–Sb alloys. The reversible capacity of composite material sample was significantly higher than carbon. Compared with the Sn–Sb alloy sample, the improvement in cycling stability has been confirmed for composite sample in this study. The reversible capacity of the composite material sample remains slightly fade after each cycle and remains above 500 mAh g^{-1} after 20 cycles at current density 50 mA g^{-1} (see the solid dot of Fig. 5). Compared with the Sn–Sb alloy, the electrochemical performance improvement of composite materials sample is evident in large current density condition. It is clear that the Sn–Sb alloy sample undergoes rapid capacity faded under the current density for 1C (see the hollow dot of Fig. 5). It remained storage capacity of 236 mAh g^{-1}, the retention capacity rate was 38% after 20 cycles. However, composite materials sample maintained a good cycle behavior. The reversible capacity drops slowly in cyclic process at the current density for 1C. It still remained storage capacity of 364 mAh g^{-1}, the retention capacity rate was 85% after 20 cycles. The unusual increase in capacity in the first few (4–5) cycles of ACSP because of the coating structure. Some of active material SnSb was isolated by amorphous carbon. In large current density condition, the electrolyte and Li^+ did not reach into the interior SnSb particle due to diffusion time not enough at the initial few cycles; some active materials are not participated in reacting. The isolated material become active as the electrolyte and Li^+ penetrates into the interior SnSb with cycling process.

Fig. 6 shows the curve of Coulombic efficiency vs. cycle number for ACSP and Sn–Sb alloy sample used as anode material for lithium-ion batteries. It can be seen that the initial efficiency of ACSP sample is not so higher and shows a larger irreversible capacity loss than other carbonous material such as graphite, which is attributed not only to the decomposition of electrolyte on the fresh surface of active particle but also to the irreversible insertion (alloying) procedure of lithium with active material because the amorphous carbon coated the surface of Sn–Sb particles is loose with plentiful micropore. The coulomb efficiency of ACSP sample becomes constant to be nearly 100% after the fifth cycle even though the initial efficiency is a little lower.

The composite material has good circulation stability, has the direct relations with its microscopic structure. Before lithium-ion insertion, the composite material consisting of Sn–Sb particles' cores covered by carbonaceous layer loose cotton-like structure. In lithium-ion insertion process, the Sn–Sb reacted electrochemically with the lithium ion to form Li_3Sb, Li_xSn and so on to squeeze amorphous carbon located the surface layer due to their volume expansion. Because the outer layer carbon is loose cotton-like structure with plentiful micropore, this micropore contracted when they were squeezed. When the lithium ion escapes, the volume Sn–Sb alloy contracted,

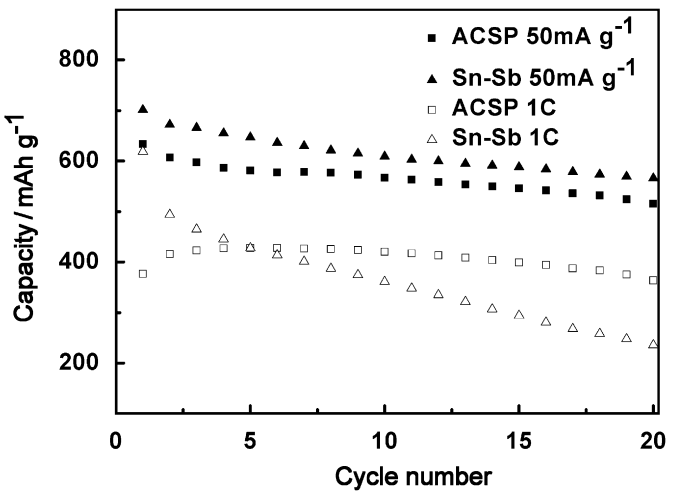

Fig. 5. Cycle capacity vs. cycle number of the ACSP and Sn–Sb alloy sample. Solid dot: current density 50 mA g^{-1}; hollow dot: current density 1C.

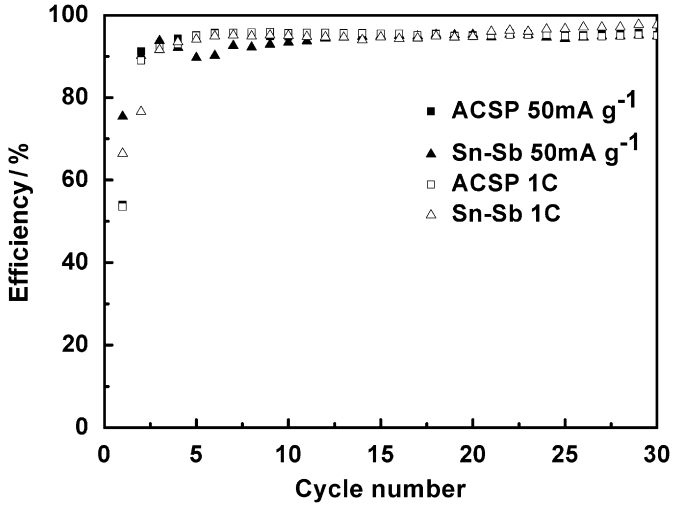

Fig. 6. Coulombic efficiency vs. cycle number of the ACSP and Sn–Sb alloy sample. Solid dot: current density 500 mAh g^{-1}; hollow dot: current density 1C.

and the outer layer carbon recoiled to the former state. This has ensured the overall volume of composite materials only changes slightly. This kind of amorphous carbonaceous materials with the loose cotton-like structure can accommodate the expansion and contraction of active materials to maintain the structure stability.

The main characteristic properties of the ACSP sample can be summarized as follows:

(a) The expansion and the contraction of active material are limited in micro capsule constructed by the carbon shell structure, which has the very stable microcosmic structure and can effectively suppress the volume effect of the Sn–Sb active particle in the charge and discharge process.
(b) Carbon shell isolated Sn–Sb active material from each other, can suppress the aggregation between the active material, which extrudes mutually to coarsen.
(c) The capacity of composite materials is much higher than that of carbon materials, because nanometer Sn–Sb material is in nuclear.
(d) Carbon plays the role of a conducting bridge among Sn–Sb particles and acts as a channel of lithium ion.

For these advantages in properties mentioned above, in theory, these composite material anodes formed in this study have a very high capacity, as well as very long cycle life.

4. Conclusion

The amorphous carbon-coated Sn–Sb particles was prepared from aqueous glucose solutions using a hydrothermal method, which shows much better cyclic performance than that of Sn–Sb alloy. It can be considered that the outer layer carbon is loose cotton-like with plentiful micropore, which can accommodate the expansion and contraction of active materials to maintain the stability of the structure.

This material showed excellent initial capacity and capacity retention with the capacity of 634 and over $500\,mAh\,g^{-1}$ after 20 cycles, respectively. The ACSP sample maintained a good cycle behavior under big current density condition. It was less affected by current density and still remained storage capacity of $364\,mAh\,g^{-1}$ and the retention capacity rate was 85% after 20 cycles. The ACSP electrode has great potential as a material for improving the energy density of a lithium secondary battery.

Acknowledgment

This work was supported by NSFC of China (Nos. 50504017, 20221101, 10335040 and 20671004).

References

[1] J.L. Tirado, Mater. Sci. Eng. R 40 (2003) 103–136.
[2] M. Wachtler, M. Winter, J.O. Besenhard, J. Power Sources 105 (2002) 151–160.
[3] J. Yang, Y. Takeda, N. Imanishi, T. Ichikawa, O. Yamamoto, Solid State Ionics 135 (2000) 175–180.
[4] J. Yang, M. Wachtler, M. Winter, J.O. Besenhard, Electrochem. Solid State Lett. 2 (1999) 161–164.
[5] K.D. Kepler, J.T. Vaughey, M.M. Thackeray, Electrochem. Solid State Lett. 2 (1999) 307–309.
[6] I. Rom, M. Wachtler, I. Papst, M. Schmied, J.O. Besenhard, F. Hofer, M. Winter, Solid State Ionics 143 (2001) 329–336.
[7] H. Li, L.H. Shi, W. Lu, L.Q. Chen, X.J. Huang, J. Electrochem. Soc. 148 (2001) A915–A922.
[8] X.D. Wu, Z.X. Wang, L.Q. Chen, X.J. Huang, Carbon 42 (2004) 1965–1972.
[9] X.D. Wu, H. Li, L.Q. Chen, X.J. Huang, Solid State Ionics 149 (2002) 185–192.
[10] L.H. Shi, H. Li, Z.X. Wang, X.J. Huang, L.Q. Chen, J. Mater. Chem. 11 (2001) 1502–1505.
[11] I. Kim, P.N. Kumta, G.E. Blomgren, Electrochem. Solid State 3 (2000) 493–496.
[12] S. Hwang, H. Lee, S. Jang, S.M. Lee, S.J. Lee, H. Baik, J. Lee, Electrochem. Solid State 4 (2001) A97–A100.
[13] K.T. Lee, Y.S. Jung, S.M. Oh, J. Am. Chem. Soc. 125 (2003) 5652–5653.
[14] F. Tiarks, K. Landfester, M. Antonietti, Langmuir 17 (2001) 908–918.
[15] Y. Liu, J.Y. Xie, J. Yang, J. Power Sources 119–121 (2003) 572–575.
[16] Y. Liu, J.Y. Xie, Y. Taked, J. Appl. Electrochem. 32 (2002) 687–692.
[17] H. Li, Q. Wang, L. H Shi, L.Q. Chen, X.J. Huang, Chem. Mater. 14 (2002) 103–108.
[18] W.X. Chen, J.Y. Lee, Z.L. Liu, Carbon 41 (2003) 959–966.
[19] W.X. Chen, J.Y. Lee, Z.L. Liu, Electrochem. Commun. 4 (2002) 260–265.
[20] X.Z. Liao, Z.F. Ma, J.H. Hu, Y.Z. Sun, X.X. Yuan, Electrochem. Commun. 5 (2003) 657–661.
[21] J.Y. Lee, R.F. Zhang, Z.L. Liu, J. Power Sources 90 (2000) 70–75.
[22] G.X. Wang, J. Yao, H.K. Liu, S.X. Dou, J.H. ahn, Electrochim. Acta 50 (2004) 517–522.
[23] G.X. Wang, J.H. Ahn, M.J. Lindsay, L. Sun, D.H. Bradhurst, S.X. Dou, H.K. Liu, J. Power Sources 97–98 (2001) 211–215.
[24] X.M. He, W.H. Pu, L. Wang, J.G. Ren, C.Y. Jiang, C.R. Wan, Electrochim. Acta 52 (2007) 3651–3653.
[25] K. Wang, X.M. He, J.G. Ren, L. Wang, C.Y. Jiang, C.R. Wan, Electrochim. Acta 52 (2006) 1221–1225.
[26] M. Noh, Y. Kwon, H. Lee, J. Cho, Y. Kim, M.G. Kim, Chem. Mater. 17 (2005) 1926–1929.
[27] X.M. He, W.H. Pu, L. Wang, J.G. Ren, C.Y. Jiang, C.R. Wan, Solid State Ionics 178 (2007) 833–836.
[28] M. Takahiro, H. Tadamitsu, O. Tomoyuki, J. Power Sources 160 (2006) 638–664.
[29] Z. Wang, W.H. Tian, X.G. Li, Acta Phys. Chim. Sin. 22 (2006) 752–755.
[30] Z. Wang, W.H. Tian, X.G. Li, J. Alloys Compds. 439 (2007) 350–354.
[31] X.M. Sun, Y.D. Li, Angew. Chem. Int. Ed. 43 (2004) 597–601.
[32] T. Sakaki, M. Shibata, T. Miki, H. Hirousue, N. Hayasshi, Bioresour. Technol. 58 (1996) 197–202.
[33] Q. Wang, H. Li, L.Q. Chen, X.J. Huang, Solid State Ionics 152–153 (2002) 43–50.
[34] Q. Wang, H. Li, L.Q. Chen, X.J. Huang, Carbon 39 (2001) 2211–2214.